Phase-Coherent Digital Communications for Underwater Acoustic Channels

Milica Stojanovic, Josko A. Catipovic, and John G. Proakis, *Fellow, IEEE*

Abstract— **High-speed phase coherent communications in the ocean channel are made difficult by the combined effects of large Doppler fluctuations and extended, time-varying multipath. In order to account for these effects, we consider a receiver which performs optimal phase synchronization and channel equalization jointly. Since the intersymbol interference in some underwater acoustic channels spans several tens of symbol intervals, making the optimal maximum-likelihood receiver unacceptably complex, we use a suboptimal, but low complexity, decision feedback equalizer. The mean squared error multiparameter optimization results in an adaptive algorithm which is a combination of recursive least squares and second-order digital phase and delay-locked loops. The use of a fractionally spaced equalizer eliminates the need for explicit symbol delay tracking.**

The proposed algorithm is applied to experimental data from three types of underwater acoustic channels: long-range deep water, long-range shallow water, and short-range shallow water channels. The modulation techniques used are 4- and 8-PSK. The results indicate the feasibility of achieving power-efficient communications in these channels and demonstrate the ability to coherently combine multiple arrivals, thus exploiting the diversity inherent in multipath propagation.

I. Introduction

THIS work is focused on achieving reliable coherent communications over underwater acoustic (UWA) channels. The motivation behind this goal is to achieve the bandwidth efficiency of coherent communications and, thus, improve the quality of existing underwater digital communication systems which commonly use noncoherent (FSK) or differentially coherent (DPSK) modulation techniques. Bandwidth efficiency is an important issue in underwater communications in various application areas such as telemetry, remote control, or speech transmission in point-to-point links and underwater networks.

The UWA channel is characterized as a time-dispersive rapidly fading channel, which in addition exhibits Doppler instabilities [1]. While vertical channels exhibit little time dispersion, horizontal channels suffer from extended multipath propagation which usually increases with range and, depending on the signaling rate, causes the intersymbol interference (ISI) to span up to several tens of symbol intervals. In some applications, unpredictable motion of the receiver and transmitter, as well as changes in the transmission medium, cause severe phase fluctuations. This is the main reason coherent communications are often not considered feasible [1]. From the viewpoint of building a robust communication receiver, the main limitation of an UWA channel is therefore the combination of time-varying multipath and phase instabilities.

Frequency-selective fading results in performance degradation of coherent reception. In recent years, much effort has been devoted to equalization of fading channels; however, the existence of perfect carrier recovery and symbol timing is often assumed. Conventionally, this estimation of receiver synchronization and equalization parameters is performed separately. Such an approach may not be well suited for rapidly changing environments. In conventional systems which employ phase and delay-locked loop (PLL, DLL) structures for synchronization, a major obstacle for satisfactory performance is the time-varying ISI [2], [3], which results in poor tracking capabilities of a synchronization subsystem. On the other hand, residual phase fluctuations impair the performance of an equalization subsystem and may cause the problem of equalizer tap rotation [4]. Therefore, the unified treatment of synchronization and equalization, justified by the fact that joint estimates are always at least as good as the marginal ones, is expected to give better results. In order to achieve the bandwidth and power efficiency of coherent communications and the diversity improvement from multipath propagation, we address the problem of joint synchronization and equalization optimization.

The optimal receiver for joint estimation of synchronization parameters and the data sequence in the case of a known and fixed channel was originally presented in [5]. It is obtained using the maximum likelihood (ML) approach. In the case of a time-varying channel, such an approach is well suited for burst-type communications when the parameters to be estimated can be considered relatively fixed over a burst. When the channel is not known and may be possibly time varying, the optimal receiver is aided by an adaptive channel estimator [6]. A major shortcoming of the optimal structure is its complexity, which grows exponentially with the length of the channel response, making it impractical for high symbol rates when the channel response spans more than ten symbol intervals. To circumvent the complexity problems which arise at high data rates and long ranges, we use a suboptimal structure which employs an adaptive decision feedback equalizer (DFE). The performance of a DFE in the absence of decision errors is comparable to that of a ML sequence estimator [7], its complexity is linear in the number of taps, and it does not rely as heavily on the assumptions about the statistical properties of the noise. The equalizer tap weights are estimated jointly with the synchronization parameters using the minimum mean

Manuscript received May 1993.

M. Stojanovic and J. G. Proakis are with the Department of Electrical and Computer Engineering, Northeastern University, Boston, MA 02115.

J. A. Catipovic is with the Department of Applied Ocean Physics and Engineering, Woods Hole Oceanographic Institution, Woods Hole, MA 02573.

IEEE Log Number 9214556.

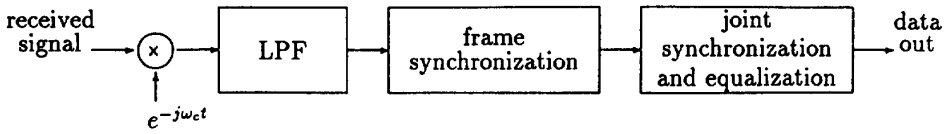

Fig. 1. Block diagram of the receiver.

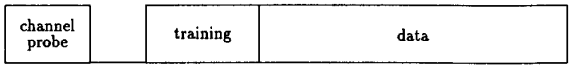

Fig. 2. Signaling frame.

squared error (MSE) criterion. Channel tracking is accomplished through the use of an adaptive algorithm which is a combination of recursive least squares (RLS) and a second-order digital PLL/DLL. The use of a fractionally spaced DFE eliminates the need for symbol timing estimation. An RLS type of algorithm provides fast tracking capabilities, which offer improved performance in the dynamic ocean medium.

The communication system structure is discussed in Section II, and the receiver algorithm is derived in Section III. The proposed algorithm has been applied successfully to the experimental data obtained from various types of horizontal UWA channels, namely long-range deep and shallow water and short-range shallow water channels. The experimental results are presented in Section IV. The experiments were conducted by the Woods Hole Oceanographic Institution (W.H.O.I.).

II. Receiver Structure

We are focusing our attention on linear modulation schemes, for which the transmitted signal is represented in its equivalent complex baseband form as:

$$u(t) = \sum_n d_n g(t - nT) \tag{1}$$

where $\{d_n\}$ are the transmitted M-ary data symbols, $g(t)$ is the basic transmitter pulse, and T is the signaling interval. This signal is modulated onto a carrier of angular frequency ω_c and transmitted over the channel. The overall block diagram of the receiver is shown in Fig. 1.

The received signal, after being brought to baseband and lowpass filtered, is frame synchronized prior to any processing. This is accomplished by matched filtering to a known channel probe. The signaling frame which contains the channel probe and the data block is shown in Fig. 2. The transmission is organized in blocks so as to provide periodic frame synchronization and retraining for the DFE.

After coarse alignment in time, the received signal is modeled as:

$$v(t) = \sum_n d_n h(t - nT - \tau)e^{j\theta} + \nu(t), \qquad t \in T_{\text{obs}} \tag{2}$$

where T_{obs} is some interval of time in which the channel parameters can be regarded as fixed, and is introduced to avoid the more complicated notation with time-dependent channel parameters. The overall channel impulse response $h(t)$ includes the physical channel and any transmit and receive filtering. Since the coarse alignment in time has been accomplished, the delay uncertainty τ is within one symbol interval. The carrier phase distortion θ is not included in the overall response, for reasons which will become apparent shortly. The term $\nu(t)$ represents additive noise.

The structure of the receiver block for joint equalization and synchronization is shown in Fig. 3. Since the channel $h(t)$ is not known, the matched filter which would be a part of the optimal receiver is omitted, and the received signal $v(t)$ is sampled directly. Sampling may be performed at the symbol rate, in which case the existence of an accurate symbol timing estimate is crucial for the satisfactory performance of the equalizer. On the other hand, a fractionally spaced equalizer, which uses sampling interval T_s smaller than the reciprocal of the signal bandwidth, is insensitive to the timing phase of the incoming signal [8], i.e., it is capable of synthesizing the optimal sampling instant provided that coarse synchronization exists. In the limiting case of an infinite number of taps, it provides both functions of matched filtering and optimal symbol-spaced equalization [7]. Due to the fact that τ is changing with time, it may be suspected that with fixed sampling times in a fractionally spaced structure of finite length, the desired portion of the received signal, which contains information on the currently detected symbol, will slip out of the feedforward equalizer. However, this phenomenon has not been observed in any of the analyzed channels with data block durations on the order of 10 s. Only if very long, or continuous, messages are being transmitted would the need arise for adaptive adjustment of the timing phase (in order to ensure the correct position of the center tap of the equalizer) [9]. Although a fractionally spaced equalizer is our choice for implementation, we include in the analysis the estimation of symbol delay, since the algorithm derivation is essentially not affected by this choice.

In some cases when symbol rate sampling is used, the existence of initial estimates of synchronization parameters within a convergence region may be needed. The initial estimates of Doppler frequency, carrier phase, and symbol delay can be obtained from a short synchronization preamble in a nonrecursive manner based on ML estimation principles. We now describe how these initial estimates are obtained; however, such a procedure is not deemed necessary if fractionally spaced equalization is used.

A. Initial Nonrecursive Estimation of Synchronization Parameters

Let the transmitted and received preamble signals be denoted by $u_p(t)$ and $v_p(t)$, respectively, with indices $_1$ and

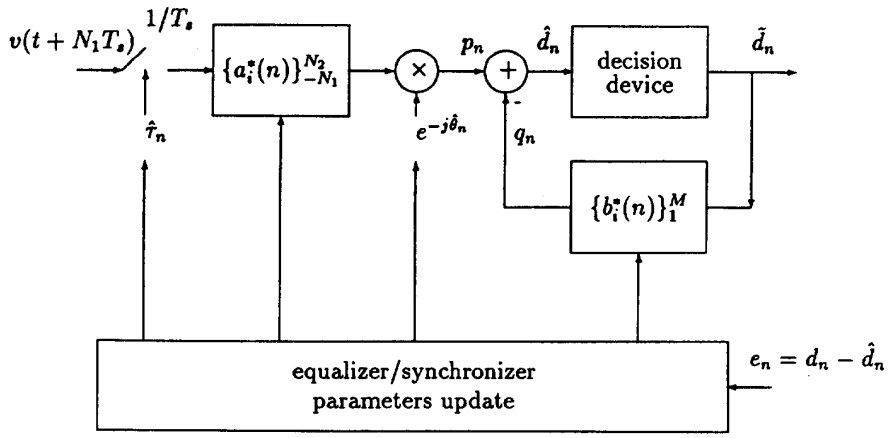

Fig. 3. Receiver structure.

2 corresponding to the parts of the preamble designed for the estimation of Doppler and timing parameters, respectively. The received signal is sampled using N_s samples per symbol interval by a free running sampler, and observed at times $t = 1, \cdots, N_pN_s$, where $N_p = N_{p_1} + N_{p_2}$ is the number of symbols in the preamble. Assuming that the additive noise is white Gaussian, the initial estimates of Doppler frequency $\hat{\omega}_d$ and the carrier phase shift $\hat{\theta}_0$ are approximately determined from:

$$\hat{\omega}_d = \arg\max_{\omega} A(\omega)$$
$$\hat{\theta}_0 = \Phi(\hat{\omega}_d) \tag{3}$$

where the amplitude $A(\omega)$ and the phase $\Phi(\omega)$ define the (discrete) Fourier transform:

$$A(\omega)e^{j\Phi(\omega)} = FT\{v_{p_1}(t)u_{p_1}^*(t)\} \tag{4}$$

which can be computed using the desired resolution. After compensating for the estimated Doppler in the received signal, the initial estimate of symbol timing $\hat{\tau}_0$ is obtained as:

$$\hat{\tau}_0 = \arg\max_{\tau=1,\cdots,N_s} \mathrm{Re}\left\{\sum_{n=0}^{N_{p_2}-1} v_{p_2}(nN_s + \tau)d_n^*\right\}. \tag{5}$$

where $\{d_n\}_0^{N_{p_2}-1}$ are the known symbols of the timing preamble. This two-step procedure approximates the more general parallel search for all synchronization parameters, provided that the residual error in timing estimation, as obtained from frame synchronization, is small.

III. Receiver Algorithm

Although theoretically the optimally chosen complex tap weights of the linear equalizer correct for any phase offset in the received signal, this is not the case in practice. The carrier phase $\theta(t)$ is a function of time and can be modeled as a sum of three terms: constant phase offset, Doppler frequency shift, and random phase jitter. While an adaptive equalizer is capable of correcting for the constant phase offset and possibly some slow variations of the carrier phase, the residual carrier frequency offset, as well as more rapid phase fluctuations, result in equalizer tap rotation. This increases the misadjustment noise, and may eventually cause the equalizer taps to diverge. Typically, the tap gains should not change by more than a few percent from one symbol interval to another [10]. Therefore, the addition of a carrier phase synchronization loop is necessary to ensure proper operation of the equalizer in the conditions of large phase fluctuations encountered in the UWA channels.

In order to take care of the ISI caused by future symbols, a delay of a certain number N_1 of sampling intervals is introduced in the received signal. The $N = N_1 + N_2 + 1$ taps of the feedforward filter are arranged in a row vector $\boldsymbol{a}'$, and the input signal samples currently stored in the feedforward equalizer are given by:

$$\boldsymbol{v}(n, \hat{\tau}) = [v(nT + N_1T_s + \hat{\tau}) \cdots v_n(nT - N_2T_s + \hat{\tau})]^T \tag{6}$$

where $(\cdot)^T$ and $(\cdot)'$ denote transpose and conjugate transpose, respectively. The feedforward equalizer output is produced once per symbol interval, and the carrier phase update is performed accordingly, yielding:

$$p_n = \boldsymbol{a}'\boldsymbol{v}(n, \hat{\tau})e^{-j\hat{\theta}}. \tag{7}$$

Carrier recovery can be moved further into the decision feedback loop, but only minor improvements are achieved in this way [10]. The feedback filter has tap weights $\boldsymbol{b}'$ and operates on the sequence of M previously detected symbols:

$$\tilde{\boldsymbol{d}}(n) = [\tilde{d}_{n-1} \cdots \tilde{d}_{n-M}]^T \tag{8}$$

to produce an estimate of the ISI caused by these symbols:

$$q_n = \boldsymbol{b}'\tilde{\boldsymbol{d}}(n). \tag{9}$$

This estimate is subtracted from the output of the linear section to obtain the overall analog estimate of the data symbol:

$$\hat{d}_n = p_n - q_n. \tag{10}$$

The decision $\tilde{d}_n$ is formed by quantizing the estimate $\hat{d}_n$ to the nearest symbol value.

The estimation error is defined as:

$$e_n = d_n - \hat{d}_n \tag{11}$$

and the optimization of the receiver parameters is performed through minimization of the MSE $= E\{|e_n|^2\}$. Differentiating the MSE with respect to all relevant parameters results in the set of gradients:

$$\frac{\partial \text{MSE}}{\partial \boldsymbol{a}} = -2\text{E}\{\boldsymbol{v}(n, \hat{\tau})e_n^*\}e^{-j\hat{\theta}} \tag{12}$$

$$\frac{\partial \text{MSE}}{\partial \boldsymbol{b}} = 2\text{E}\{\tilde{\boldsymbol{d}}(n)e_n^*\} \tag{13}$$

$$\frac{\partial \text{MSE}}{\partial \hat{\theta}} = -2\,\text{Im}\{\text{E}\{p_n(d_n + q_n)^*\}\} \tag{14}$$

$$\frac{\partial \text{MSE}}{\partial \hat{\tau}} = -2\,\text{Re}\{\text{E}\{\dot{p}_n e_n^*\}\} \tag{15}$$

where, in the last equation, $\dot{p}_n = \boldsymbol{a}'\dot{\boldsymbol{v}}(n, \hat{\tau})e^{-j\hat{\theta}}$ is the output of the feedforward section with the corrected phase, when its input is the time derivative of the received signal $\dot{v}(t)$. In the decision-directed mode, d_n should be substituted by $\tilde{d}_n$. Setting the gradients equal to zero results in the set of equations whose solution represents the jointly optimal receiver parameters. Since the optimal values of the receiver parameters are actually time varying, we seek to obtain a solution to the system of equations in a recursive manner. Then, it can be expected that once the algorithm has converged, it will continue to track the time variations of the channel. A commonly used form of an adaptive algorithm is based on stochastic gradient approximation, whose simplest form is the so-called one shot approximation algorithm [5], [6], in which each parameter is updated by the amount proportional to the instantaneous estimate of its gradient. It represents a combination of a simple least mean squares (LMS) update for the equalizer tap weights and a first-order digital PLL/DLL for synchronization parameters tracking. Such an algorithm, however, may not be powerful enough to track all the fluctuations present in the UWA channel.

To make this type of algorithm robust with respect to time variations of the UWA channel, we introduce several modifications. To obtain the necessary tracking capabilities of the carrier phase estimate, a second-order update equation for this parameter is needed [11]. It is obtained by recognizing that the gradient of the MSE with respect to the carrier phase estimate represents the output of an equivalent phase detector. Based on the analogy with the digital PLL [12] but using the expression (14), the equivalent phase detector output is defined as:

$$\Phi_n = \text{Im}\{p_n(d_n + q_n)^*\}. \tag{16}$$

The second-order carrier phase update equation is then given by:

$$\hat{\theta}_{n+1} = \hat{\theta}_n + K_{f_1}\Phi_n + K_{f_2}\sum_{i=0}^{n}\Phi_i \tag{17}$$

where K_{f_1}, K_{f_2} are the proportional and integral tracking constants. The second-order timing phase update can be obtained analogously. While these update equations correspond to perfect loop integration, it is also possible to use imperfect integration as well as sliding window integration. In the absence of ISI and decision errors, the update equations for the synchronization parameters describe the operation of classical second-order synchronization loops. Here, however, they are coupled with the process of equalization.

To achieve faster convergence of the algorithm during relatively short training periods, we use the RLS estimation criterion for the equalizer tap weights update. Besides allowing for shorter training periods, fast convergence is advantageous on rapidly changing channels since it enables the receiver to make full use of only temporarily present multipath components. An RLS algorithm [13], applied to the composite data vector

$$\boldsymbol{u}'(n) = [\boldsymbol{v}'(n, \hat{\tau})e^{j\hat{\theta}}\tilde{\boldsymbol{d}}'(n)] \tag{18}$$

adaptively estimates the overall equalizer vector $\boldsymbol{c}'(n) = [\boldsymbol{a}'(n) - \boldsymbol{b}'(n)]$, which has a closed-form MMSE solution

$$\boldsymbol{c} = [E\{\boldsymbol{u}(n)\boldsymbol{u}'(n)\}]^{-1}E\{\boldsymbol{u}(n)d_n^*\}. \tag{19}$$

To accommodate for the time variations of the channel, the RLS forgetting factor λ, which accounts for the exponential windowing of the data, must be taken less than 1.

While the structure of the receiver allows carrier recovery to take place after equalization, thus eliminating the problem of the delay in phase estimate [4], this is not the case with symbol delay estimation. The estimate $\hat{\tau}_n$ lags behind the true timing phase $\tau(nT + N_1T)$, producing residual timing jitter. This is additional motivation to use a fractionally spaced equalizer, which, being insensitive to the choice of the sampling instant, automatically overcomes this problem. If a fractional spacing of $T/2$ is used, which is sufficient for signals bandlimited to $1/T$, the receiver algorithm requires only two samples per symbol interval. Since no feedback to the analog part of the receiver is required, it is well suited for an all-digital implementation.

Various fast implementations of the RLS algorithm exist, and the numerically stable algorithm presented in [14] was found to be well suited for the fractionally spaced DFE. The complexity of this algorithm is $10N$, and there are practically no limitations for its application in the UWA communications where data rates are very low as compared to the currently available processing speeds.

It is known that multipath propagation in fading channels offers performance improvement similar to that of explicit diversity combining [15]. The proposed receiver attempts to achieve this improvement by synchronously combining multiple signal arrivals, which is made possible by the process of joint Doppler synchronization and adaptive equalization.

IV. Experimental Results

The proposed algorithm has been applied to experimental data obtained from various types of UWA channels, and some of the results are presented in this section. The experiments

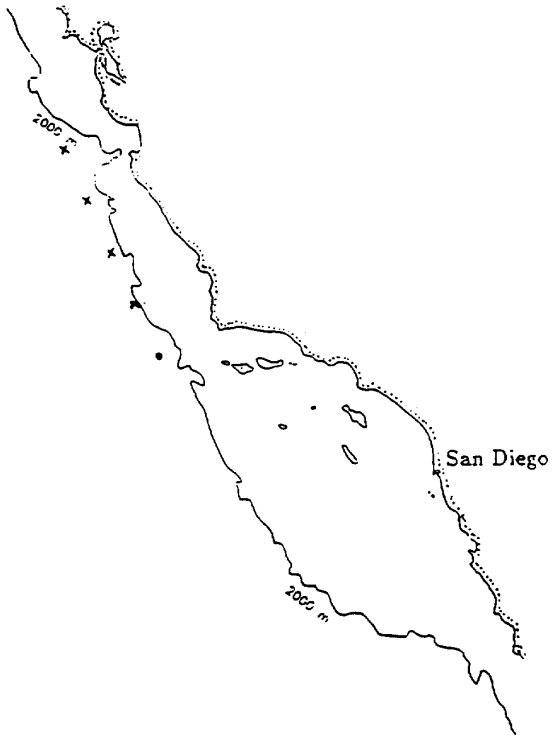

Fig. 4. Deep water long-range experiment site.

Fig. 5. Shallow water long-range experiment site.

were performed in long-range deep and shallow water and in short-range shallow water channels.

Propagation in deep water occurs in convergence zones, and is characterized by deep fades but relatively stable finite multipath. Long-range shallow water channel is characterized by longer multipath, which is less stable than that observed in deep water since propagation in shallow water is more affected by random bottom and surface reflections. Finally, short-range shallow water propagation suffers from the surface time variability which results in faster changes of the propagation conditions than those observed in any of the long-range channels. All three types of channels exhibit considerable random phase fluctuations.

A. Experiment Descriptions

The experiment in deep water was performed off the coast of California in January 1991. Fig. 4 shows the position of the receiver ship and several positions of the transmitter ship. The transmission ranges were 40–140 nautical miles, with reception occurring at the 1st, 2nd, 3rd, and 4th convergence zones. Transmitter power was 193 dB re μPa, and carrier frequency of 1 kHz was used. The transducer was attached to the stern frame of the ship and deployed 100 m below the surface. The receiver array consisted of 32 omnidirectional sensors spanning depths from 375 to 1750 m.

The long-range shallow water experiment was performed at the New England Continential Shelf in May 1992, with the receiver and transmitter ships positioned as shown in Fig. 5. The receiver was anchored in approximately 40–50 m deep water and had a vertical array of 20 omnidirectional sensors at depths of 15–35 m. Transmission ranges were 15–65 nautical miles. The transmitter power and carrier frequency were the same as in the deep water experiment.

The symbol rates used in both long-range experiments were 33, 100, 333, and 1000 symbols per second (s/s), and 200 and 500 s/s in the shallow water experiment. The modulation formats were QPSK and 8-PSK.

Fig. 6 shows the setting for the shallow water experiment, performed in Buzzards Bay in February 1991. Transmitter power of 183 dB re μPa was used, and the carrier frequency was 15 kHz. The signals were transmitted over ranges of approximately 1–4 nautical miles. The transmitter was deployed 7–10 m below the surface, in about 17 m deep water. The receiver employed one directional hydrophone at a depth of 3.5 m, and two omnidirectional hydrophones submerged at 3.5 and 7 m. The symbol rates for this experiment were 500–10000 s/s, and the modulation technique was QPSK.

The signaling format of Fig. 2 was used. The channel probe consisted of a 13-element Barker code of unshaped (rectangular) pulses in the long-range experiments, and of a single pulse in the short-range experiment. In all of the experiments, the data block signals were shaped at the transmitter by a cosine roll-off filter with roll-off factor 0.5 and truncation length of ± 2 symbol intervals. The data were maximum-length shift register pseudonoise sequences. Signal design details are given in [16].

B. Channel Characterization

To gain insight into the general channel characteristics prior to receiver design, a series of adaptive channel estimation experiments was performed. Adaptive channel estimation, representing in essence the same problem as adaptive equalization, was accomplished by incorporating the phase tracking loop into the channel estimator, in a manner described in Section III. Besides showing the multipath structure of a

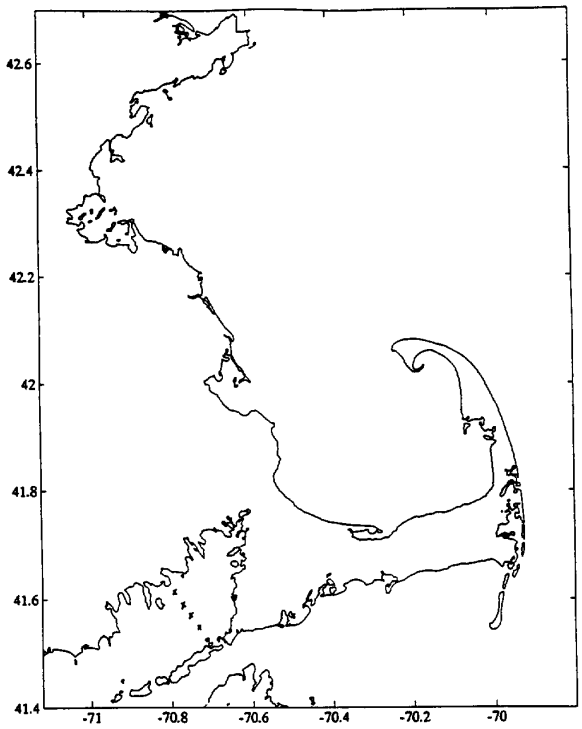

Fig. 6. Shallow water short-range experiment site.

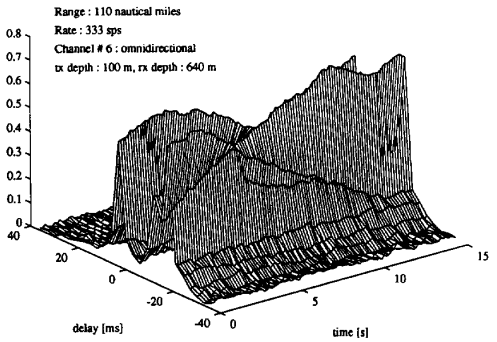

Fig. 7. Ensemble of channel responses: Long-range deep water.

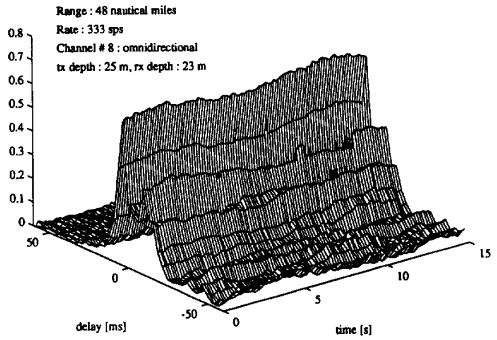

Fig. 8. Ensemble of channel responses: Long-range shallow water.

particular channel, adaptive channel estimation also shows the time variation of the channel impulse response.

Fig. 7 shows an ensemble of channel impulse responses obtained on a representative long-range deep water channel at 110 nautical miles (channel 6). The channel number refers to the hydrophone of the array, 0 being the one closest to the surface. The channel responses as a function of delay are stacked in time, with time intervals of 150 ms between each two responses shown. The total delay shown in the figure is 75 ms, indicating a multipath delay spread of about 60 ms in this channel. For signaling at 30 s/s, this means that the ISI spans two symbols; for signaling at 300 s/s, it may extend up to 20 symbols. The total time span shown in Fig. 7 is 15 s, and the channel is clearly not constant in this interval of time. Its coherence time is on the order of a couple of seconds. Note also the behavior of the principal arrival, i.e., the one with the largest energy. It is not always the same arrival that has the largest energy, which makes it possible to have more than one principal arrival in this channel. In general, this is typically a nonminimum phase channel while there are also cases of strictly maximum phase channels, depending on the range, depth, and given sound speed profile.

As opposed to deep water, where the channel response can be well approximated as having finite duration, the shallow water long-range channel suffers from extended multipath which is due to random reflections from the sea bottom and the surface. An example is shown in Fig. 8 for the range of 48 nautical miles (channel 8). The total delay shown in this figure is 120 ms, over which we observe the characteristic ringing of the channel. Regardless of the fact that the energy of individual arrivals is much smaller than that of the main arrival, all of this long ringing contributes to the overall ISI and has to be taken care of by the equalizer. The principal arrival in this channel is fairly stable, and although a single principal arrival is present in this example, this is not generally the case. A strong second reflection may be observed, depending on the receiver depth at a given range. This is again a nonminimum phase channel. However, the causal part of its response is typically much longer than that preceding the main arrival. As opposed to the main arrival, the reverberation is fairly unstable.

Fig. 9 shows the ensemble of channel responses obtained at two nautical miles in the shallow waters of Buzzards Bay. This is an example of a more rapidly varying channel. Fig. 10 shows the same channel but with higher multipath resolution and indicates a delay spread of about 5 ms. The multipath spread generally increases slightly with range. The short-range channel is a nonminimum phase channel with unstable principal arrival.

The observed channel properties are summarized in Table I. The results of channel estimation are used to determined receiver parameters, such as the number of equalizer tap weights and the forgetting factor of the RLS algorithm.

C. Performance Results

We now turn our attention to the performance results of the proposed algorithm for joint carrier synchronization

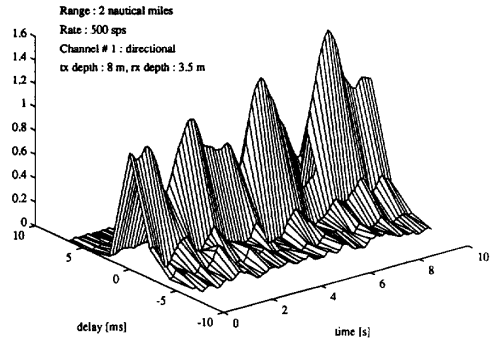

Fig. 9. Ensemble of channel responses: Short-range shallow water.

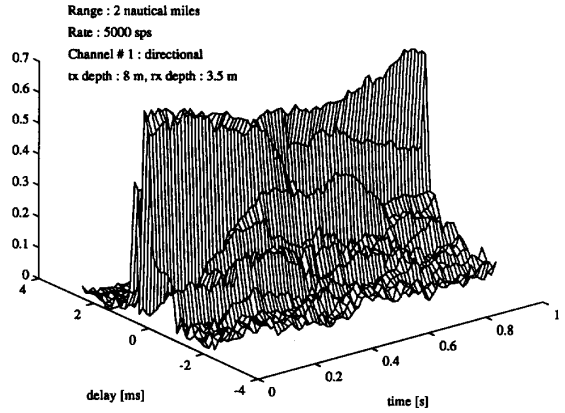

Fig. 10. Ensemble of channel responses: Short-range shallow water.

TABLE I

	taps $(N+M)$ at max. rate	typical Doppler	phase variation	K_f, f_1	RLS f.f.	no errors in 10^4, QPSK
long r. deep w.	80+30	~ 0.1 *Hz*	$< 0.5\frac{rad}{s}$	0.3	0.99	333 *sps* 110 naut.mi.
long r. shallow w.	100+80	~ 0.001 *Hz*	$< 1\frac{rad}{s}$	1	0.995	500 *sps* 48 naut.mi.
short r. shallow w.	80+40	~ 1 *Hz*	$< 5\frac{rad}{s}$	2.5	0.98-0.99 (critical)	5 *ksps* 2 naut.mi.

and fractionally spaced DFE on the previously mentioned channels. Issues concerning the impact of channel structure and dynamics are also discussed.

Fig. 11 shows the results obtained with QPSK signals transmitted at the rate of 33 s/s over 80 nautical miles (two convergence zones). Shown in the upper part are the snapshot of the channel impulse response as obtained from the channel probe, and the scatter plot of the received signal after the constant Doppler frequency shift has been removed. Although there is not much time dispersion here, the input scatter plot is somewhat smeared mainly due to the phase fluctuations. Performance of the detection algorithm is shown in terms of its mean squared error, which indicates convergence of the

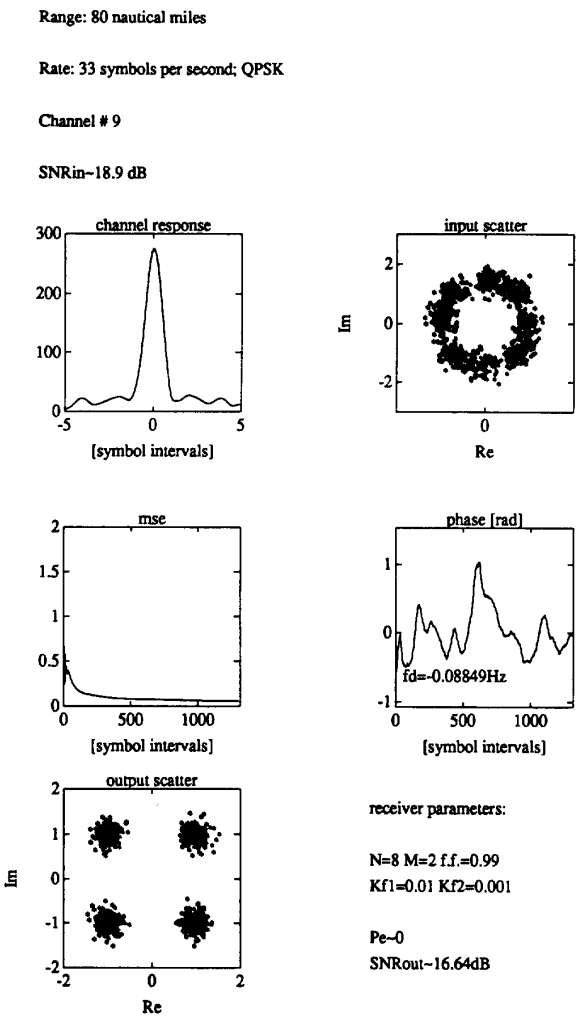

Fig. 11. Long-range deep water: Omnidirectional receiver at 780 m depth.

algorithm, the carrier phase estimate, and an output scatter plot. The carrier phase estimate, which is given in radians as a function of time measured in symbol intervals, indicates that significant phase variations occur in intervals of only couple of symbols. The scatter plot of the estimated data symbols on which the decisions are performed shows a completely open eye pattern, and there were no errors detected in this case in the block of 1000 symbols. The values of the receiver parameters are indicated in the figure. The equalizer had $N = 8$ $T/2$ spaced feedforward taps and $M = 2$ feedback taps. The fractional spacing of $T/2$ was used in all the cases, since it is sufficient for the signal bandwidth $3/4T$. The proportional carrier phase tracking constant was $K_{f_1} = 0.01$. We have found that the choice of the integral phase tracking constant, ten times smaller than the proportional tracking constant, always resulted in satisfactory performance. The forgetting factor of the RLS algorithm was chosen by trial to be $\lambda = 0.99$.

Fig. 12 presents results for a QPSK signal transmitted at the rate 333 s/s over 110 nautical miles (three convergence

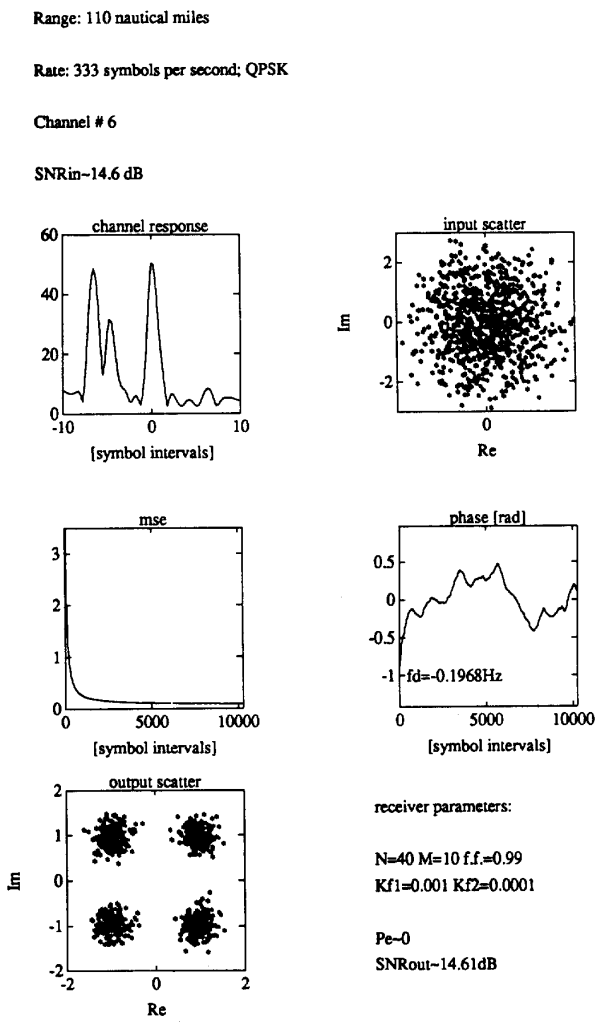

Fig. 12. Long-range deep water: Omnidirectional receiver at 645 m depth.

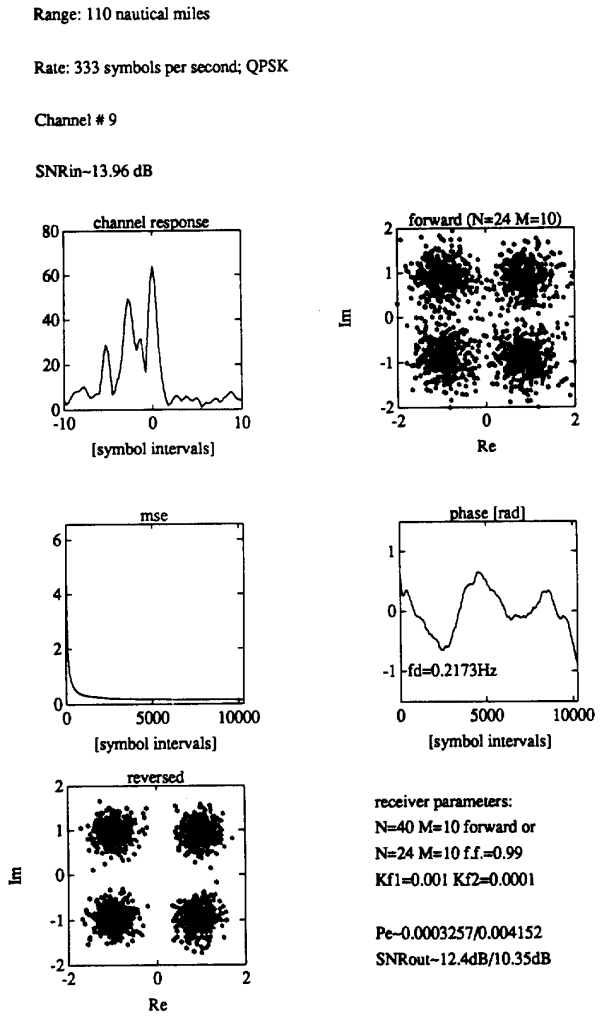

Fig. 13. Long-range deep water: Omnidirectional receiver at 780 m depth.

zones). This is the same channel (channel 6) whose time evolution was shown in Fig. 7. The input scatter plot in this case is completely smeared due to the strong multipath, phase fluctuations, and noise. The algorithm successfully copes with both ISI and phase variations, as can be seen from the output scatter plot. $P_e \sim 0$ indicates that no errors were detected in 10,000 symbols. Note that since constant transmitter power was used for all transmissions, the input SNR, whose value as measured from the channel probe is indicated in each figure, is lower for higher data rates.

It is worth mentioning that strong ISI encountered on this channel actually yielded better performance than with other channels at the same range which did not exhibit the double main arrival structure. This can be seen by comparing the output SNR's which are defined as:

$$\mathrm{SNR}_{\mathrm{out}} = 10\log\frac{|d_n|^2}{\frac{1}{N_d}\sum_1^{N_d}\left|d_n - \hat{d}_n\right|^2} \tag{20}$$

with N_d the number of data symbols in a block. This fact demonstrates the ability of the receiver to exploit multipath propagation. An example of transmission at the same rate and range, but using a different array sensor, is given in Fig. 13. This is an interesting example of a channel which exhibited a maximum phase response. In this case, a certain reduction in the equalizer complexity can be achieved by simply reversing the time of the received signal. If the received signal samples are stored prior to processing and equalization then performed backwards in time, the channel impulse response, as seen by the equalizer, will be minimum phase. This allows a shorter feedforward section, which is essentially responsible for elimination of the ISI due to future symbols, as well as more effective performance of the feedback section [17]. Fig. 13 shows the output signal scatter plot obtained with normal mode equalization and $N = 24$ (upper right corner), and that of the reversed mode equalization and $N = 24$ only. Of course, similar performance can be achieved in a normal mode

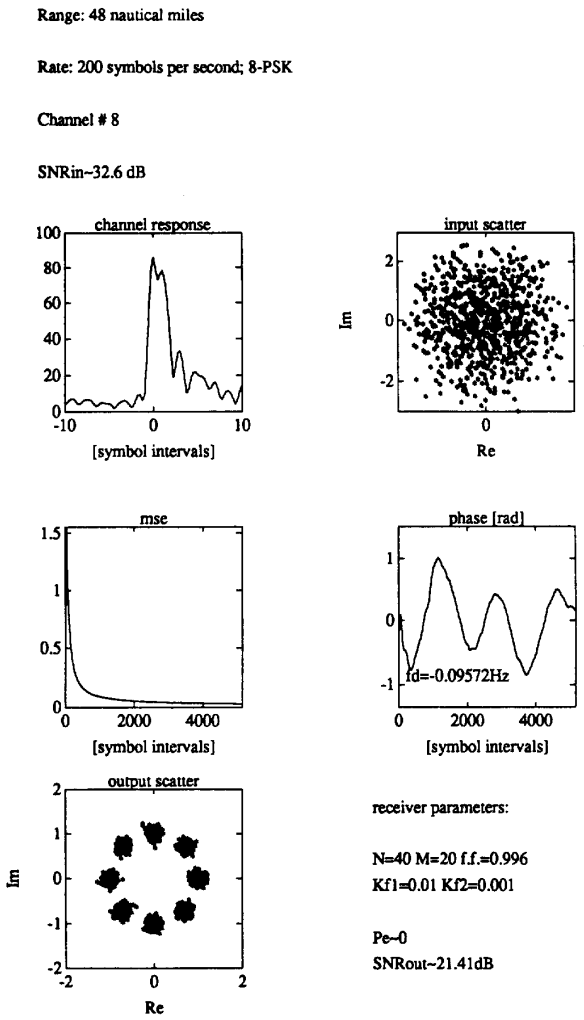

Fig. 14. Long-range shallow water: Omnidirectional receiver at 23 m depth.

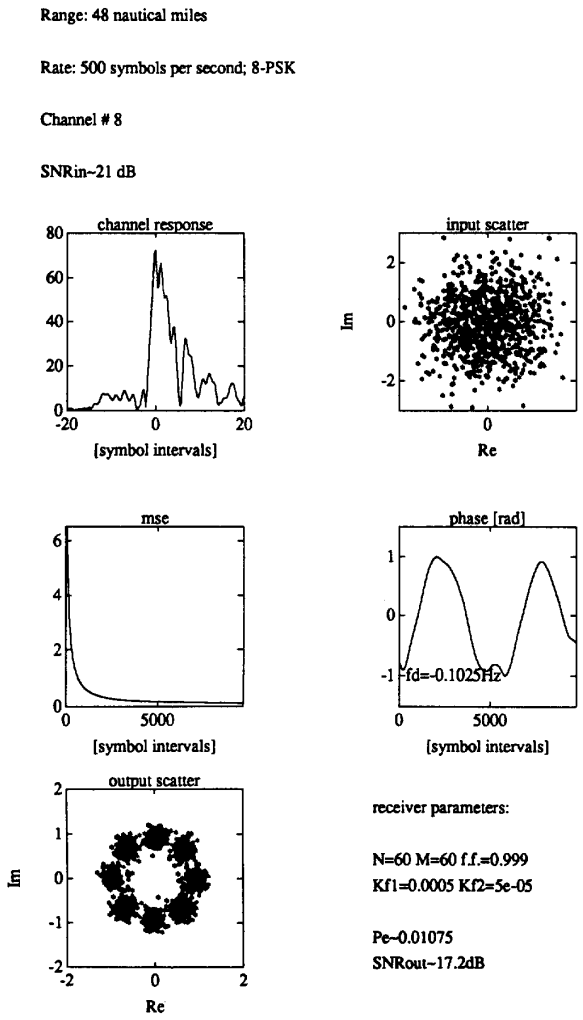

Fig. 15. Long-range shallow water: Omnidirectional receiver at 23 m depth.

with $N = 40$, but this is done mainly by linear equalization. The estimated symbol error probabilities and output SNR's are indicated for reversed and normal mode equalization, respectively.

An attempt was made to demodulate data transmitted over 140 nautical miles (four convergence zones), but it was not successful at higher data rates. The observed SNR's were only on the order of few dB, and we believe that the incorrect positioning of the receiver ship, possibly close to a shadow zone, is one of the reasons for this. In order to gain full advantage of multipath propagation, correct receiver positioning is a critical issue in a long-range deep water channel. This argument is supported by the fact that somewhat better performance was obtained at 110 nautical miles than at 80 nautical miles, although the attenuation increases with distance.

Next we show some of the results for the shallow water long-range channel. Figs. 14 and 15 refer to 8-PSK transmission over 48 nautical miles, channel 8. At 200 s/s, the receiver achieves error-free performance in 10,000 symbols. When the data rate is increased to 500 s/s, the output scatter plot shows that the performance becomes saturated due to the increased noise level. The estimated probability of symbol error in this case is on the order of 10^{-2}. However, these signals were trellis coded at the transmitter by a 2/3 Ungerboeck code, and there were no errors detected in this block of data after subsequent decoding was performed on the sequence of estimated data symbols.

This brings us to the question of performance limitations of the proposed algorithm and the example of QPSK transmission at 1000 s/s shown in Fig. 16. In this case, $N = 100$ feedforward and $M = 80$ feedback taps were needed to deal with the extended ISI. Although the mean squared error and the output scatter plot indicate the convergence of the algorithm, the quality of performance with probability of error estimated to be on the order of 10^{-3} may not be satisfactory. The basic reasons for the limitations of the proposed algorithm encountered at high data rates lie in the fact that, with

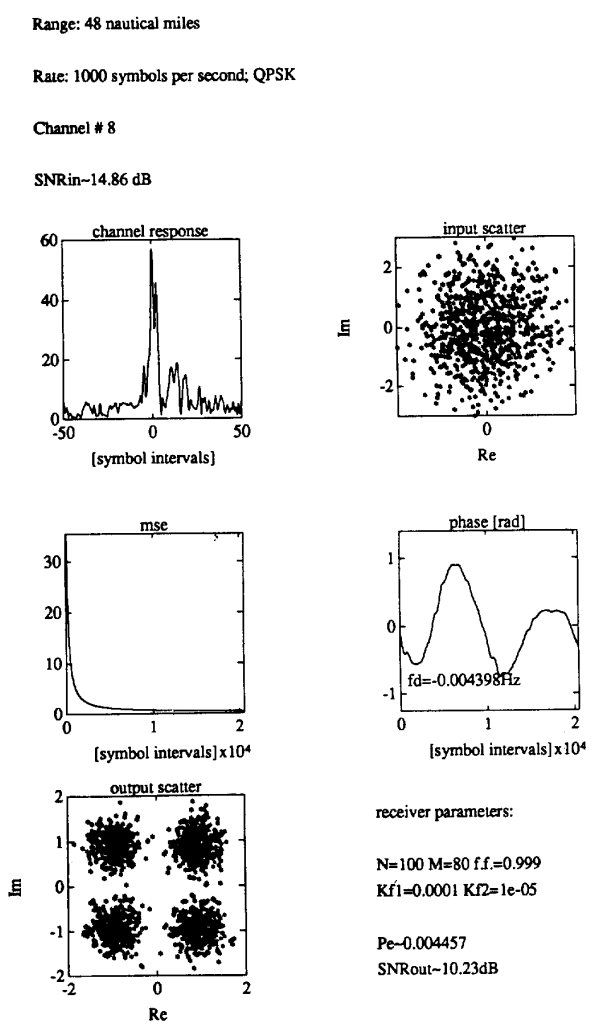

Fig. 16. Long-range shallow water: Omnidirectional receiver at 23 m depth.

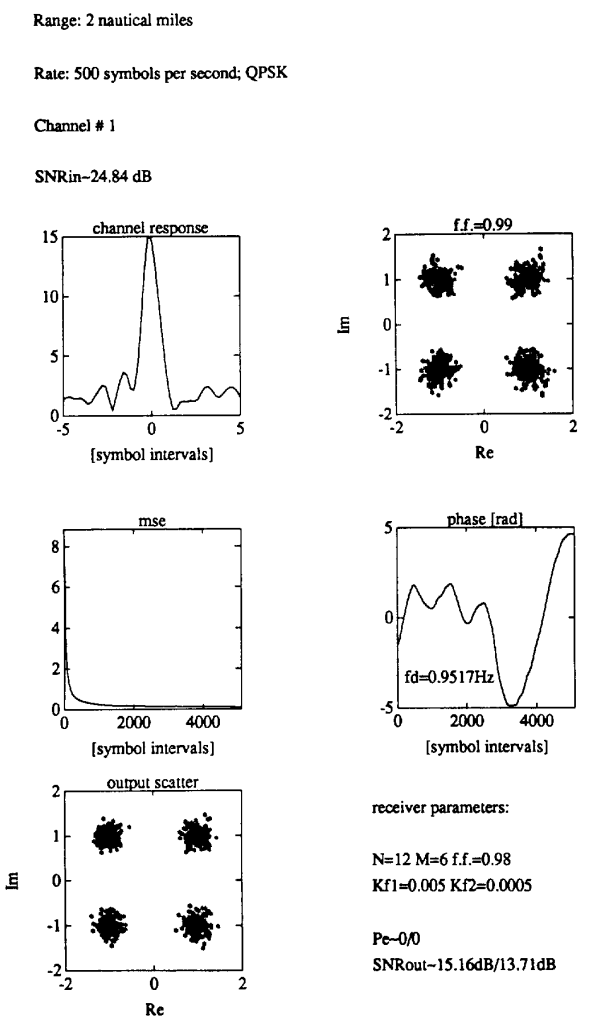

Fig. 17. Short-range shallow water: Directional receiver at 3.5 m depth.

constrained transmitter power, noise levels are higher while, at the same time, multipath (as measured in the number of symbol intervals) is longer. Longer channel responses require longer equalizers, which in turn result in higher noise enhancement. An open area of research is finding the ways of reducing the equalizer lengths and, therefore, increasing the equalizer capability by virtue of reducing its noise enhancement.

Another potential limitation to successful communications in the UWA channel is thought to be in its often large dynamics. As it was seen, of all the analyzed channels, the short-range shallow water channel exhibits most rapid time variations. Fig. 17 shows results for transmission over two nautical miles in this channel, at the data rate of 500 s/s, which, as the lowest data rate used, is most likely to suffer from rapid channel changes. Although quite sensitive to the choice of the RLS forgetting factor, the algorithm performs very well in this channel. The upper right corner scatter plot refers to $\lambda = 0.99$, while an improvement of 2 dB in the output SNR is achieved by reducing the forgetting factor to $\lambda = 0.98$, thus keeping up with the highly dynamic nature of this channel.

Finally, Fig. 18 shows the results obtained on the same channel but with a 5000 s/s signaling rate. The choice of $\lambda = 0.99$ was found to be adequate, and satisfactory results were also obtained at three nautical miles. At four nautical miles, performance was degraded due to lower received SNR.

Although the number of receiver parameters to be determined for each channel type is very low (equalizer length, phase tracking constants, and RLS forgetting factor), their proper choice may greatly improve the algorithm performance. Table II summarizes the more interesting numbers concerning receiver design for a particular channel type. The general rule for the number of equalizer taps is that the feedforward section should span all of the significant part of the channel response, but not much more in order to avoid noise enhancement. The length of the feedback section need not be larger than the causal ISI. The number of equalizer taps determines the length of training, which should be at least twice the total number of

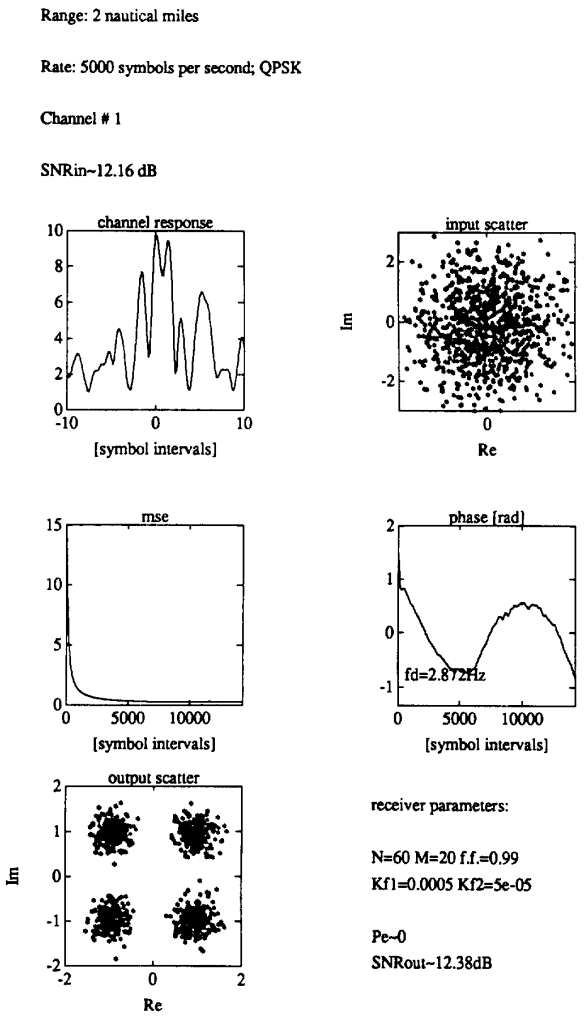

Fig. 18. Short-range shallow water: Directional receiver at 3.5 m depth.

TABLE II

	channel structure	principal arrival	channel dynamics	delay spread	receiver position
long r. deep w.	nonmin. phase (possibly max.)	> 1 unstable	moderate	60 *ms* (110 naut.mi.)	critical
long r. shallow w.	≈ min. phase	> 1 stable	moderate	100 *ms* (48 naut.mi.)	no
short r. shallow w.	nonmin. phase	1 unstable	rapid	5 *ms* (3 naut.mi.)	no

taps used. As for the carrier phase tracking constants, they can be taken inversely proportional to the symbol rate. The factors of proportionality used for the three channels are listed in Table II.

Finally, we list those maximal bit rate/range combinations where very good PSK performance was achieved (no errors detected in 10,000 symbols):

- long-range deep water: 110 nautical miles, 660 b/s
- long-range shallow water: 48 nautical miles, 1000 b/s
- short-range shallow water: 2 nautical miles, 10 kb/s

Although the sound propagation mechanism is different in the analyzed channels, the obtained results indicate that the single, relatively simple but carefully designed receiver is capable of achieving very good performance on all three types of channels.

V. Conclusion

In order to achieve reliable coherent communications over UWA channels, we have devised a receiver which jointly performs carrier synchronization and fractionally spaced decision feedback equalization of the received signal and whose parameters are adaptively adjusted using a combination of the RLS algorithm and second-order digital PLL.

The algorithm was applied to experimental data transmitted over long-range deep and shallow water, and short-range shallow water channels using PSK modulations at rates up to 1 ks/s at long and up to 10 ks/s at short ranges. The results assert the feasibility of high-speed coherent communications over these channels, and demonstrate the possibility of synchronously combining multiple signal arrivals. The presented receiver, thus, has the potential to exploit diversity inherent in multipath propagation.

While the structure of the DFE is a classical one, the concept of joint synchronization and equalization is readily extendible to various other equalization strategies which may have more potential to deal with the special structure of the UWA channel. In particular, further improvement in performance with respect to fading and noise can be achieved through the use of spatial diversity. Both the receiver structure and its algorithm allow extension to a multichannel configuration which will provide coherent MMSE spatial diversity combining. The analysis of this algorithm is deferred to a later publication.

References

[1] J. Catipovic, "Performance limitations in underwater acoustic telemetry," *IEEE J. Oceanic Eng.* vol. OE-15, pp. 205–216, July 1990.
[2] S. Hinedi and W. Lindsey, "ISI effects on BPSK and QPSK carrier tracking loops," *IEEE Trans. Commun.*, vol. COM-38, pp. 1670–1676, Oct. 1990.
[3] R. Iltis and A. Fuxjaeger, "A digital DS spread spectrum receiver with joint channel and Doppler shift estimation," *IEEE Trans. Commun.*, vol. COM-39, pp. 1255–1265, Aug. 1991.
[4] D. Falconer, "Jointly adaptive equalization and carrier recovery in two dimensional digital communication systems," *Bell Syst. Tech. J.*, vol. 55, pp. 317–334, Mar. 1976.
[5] H. Kobayashi, "Simultaneous adaptive estimation and decision algorithms for carrier modulated data transmission systems," *IEEE Trans. Commun.*, vol. COM-19, pp. 268–280, June 1971.
[6] G. Ungerboeck, "Adaptive maximum likelihood receiver for carrier modulated data-transmission systems," *IEEE Trans. Commun.*, vol. COM-22, pp. 624–636, May 1974.
[7] J. Proakis, *Digital Communications.* New York: McGraw-Hill, 1989.
[8] R. Gitlin and S. Weinstein, "Fractionally spaced equalization: An improved digital transversal equalizer," *Bell Syst. Tech. J.*, vol. 60, pp. 275–296, Feb. 1981.
[9] G. Ungerboeck, "Fractional tap spacing equalizer and consequences for clock recovery in data modems," *IEEE Trans. Commun.*, vol. COM-24, pp. 856–864, Aug. 1976.
[10] S. Prasad and S. Pathak, "Jointly adaptive decision feedback equalization and carrier recovery in digital communication systems," *AEÜ*, vol. 43, pp. 135–143, 1989.

[11] D. Godard, "A 9600 bit/s modem for multipoint communications systems," in *Proc. Nat. Telecommun. Conf.*, pp. B3.3.1–B3.3.5, New Orleans, LA, 1981.
[12] W. Lindsey and C. Chie, "A survey of digital phase-locked loops," *IEEE Trans. Commun.*, vol. COM-69, pp. 410–431, Apr. 1981.
[13] S. Haykin, *Adaptive Filter Theory.* Englewood Cliffs, NJ; Prentice Hall, 1986.
[14] D. Slock and T. Kailath, "Numerically stable fast transversal filters for recursive least squares adaptive filtering," *IEEE Trans. Signal. Proces.*, vol. 39, pp. 92–114, Jan. 1991.
[15] P. Monsen, "Theoretical and measured performance of a DFE modem on a fading multipath channel," *IEEE Trans. Commun.*, vol. COM-25, pp. 1144–1153, Oct. 1977.
[16] J. Catipovic, L. Freitag, and G. Sandsmark, "Underwater acoustic telemetry feasibility test report," W.H.O.I.-91-38 Tech. Rep., Woods Hole, MA, Nov. 1991.
[17] S. Ariyavisitakul, "A decision feedback equalizer with time-reversal structure," *IEEE J. Select. Areas Commun.*, vol. 10, pp. 599–613, Apr. 1992.

Milica Stojanovic received the Dipl. ing. degree in electrical engineering from the University of Belgrade, Belgrade, Yugoslavia, in 1988, and the M.S. degree in electrical engineering from the Northeastern University, Boston, MA, in 1991.

She is a Research Assistant at the Northeastern University, Boston, MA, where she is working towards the Ph.D. degree in electrical engineering. Her research interests include digital communications for fading multipath channels and related problems in underwater acoustics.

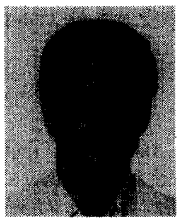

Josko A. Catipovic received the B.S. degree in electrical engineering and the B.S. degree on ocean engineering from the Massachusetts Institute of Technology, Cambridge, MA, in 1981, where he also received the Sc.D. degree in oceanographic engineering in 1987.

He is currently an Associate Scientist in the Department of Applied Ocean Physics and Engineering, Woods Hole Oceanographic Institution, Woods Hole, MA. His research interests include underwater data transmission, acoustic channel modeling, acoustic imaging, and applications of estimation and information theory to ocean engineering problems.

John G. Proakis (S'58-M'62-SM'82-F'84) received the E.E. degree from the University of Cincinnati in 1959, the S.M. degree in electrical engineering from the Massachusetts Institute of Technology, Cambridge, in 1961, and the Ph.D. degree in engineering from Harvard University, Cambridge, in 1966.

From June 1959 to September 1963 he was associated with MIT, first as a Research Assistant and later as a Staff Member at the Lincoln Laboratory, Lexington, MA. During the period of 1963–1966 he was engaged in graduate studies at Harvard University, where he was a Research Assistant in the Division of Engineering and Applied Physics. In December 1966 he joined the Staff of the Communication Systems Laboratories of Sylvania Electronic Systems, and later transferred to the Waltham Research Center of General Telephone and Electronics Laboratories, Inc., Waltham, MA. Since September 1969 he has been with Northeastern University, Boston, MA, where he holds the rank of Professor of Electrical Engineering. From July 1982 to June 1984 he held the position of Associate Dean of the College of Engineering and Director of the Graduate School of Engineering. Since July 1984 he has been Chairman of the Department of Electrical and Computer Engineering. His interests have centered on digital communications, spread spectrum systems, system modeling and simulation, adaptive filtering and digital signal processing. He is the author of the book, *Digital Communication* (New York: McGraw-Hill, 1983, 1989, second edition), and the coauthor of the book, *Introduction to Digital Signal Processing* (New York: Macmillan, 1988).

Dr. Proakis has served as an Associate Editor for the IEEE TRANSACTIONS ON INFORMATION THEORY (1974–1977), and the IEEE TRANSACTIONS ON COMMUNICATIONS (1973–1974). He has also served on the Board of Governors of the Information Theory Group (1977–1983), is a Past Chairman of the Boston Chapter of the Information Theory Group, is a Registered Professional Engineer in the State of Ohio, and is a member of Eta Kappa Nu, Tau Beta Pi, and Sigma Xi.